International Journal of Pharmaceutics 629 (2022) 122363

Contents lists available at ScienceDirect

International Journal of Pharmaceutics

journal homepage: www.elsevier.com/locate/ijpharm

3D printed biodegradable multifunctional implants for effective breast cancer treatment

Matteo Di Luca [a,b], Clare Hoskins [c], Francesca Corduas [a,d], Rachel Onchuru [c], Adeolu Oluwasanmi [c], Davide Mariotti [d], Bice Conti [b], Dimitrios A. Lamprou [a,*]

[a] School of Pharmacy, Queen's University Belfast, 97, Lisburn Road, Belfast BT9 7BL, UK
[b] Department of Drug Sciences, University of Pavia, Viale Taramelli, 12, 27100 Pavia, Italy
[c] Department of Pure and Applied Chemistry, Technology Innovation Centre, University of Strathclyde, 99, George Street, Glasgow G1 1RD, UK
[d] Nanotechnology and Integrated Bio-Engineering Centre (NIBEC), Ulster University, Jordanstown Campus – Newtownabbey, BT37 0QB, UK

ARTICLE INFO

Keywords:
Additive manufacturing
Bioprinting
Breast cancer
Au Nanoparticles
5-Fluorouracil
Biodegradable implants

ABSTRACT

By carefully controlling the dose administered and the drug release rate from drug-eluting implants, safety and efficacy of the therapeutic agent dispensed can be improved. The present work focuses on the promising advantages of 3D Bioprinting process in developing two layers' implantable scaffolds. The two layers have different functions, in order to ensure a more effective and synergistic breast cancer therapy. First layer involves use of polymers such as Poly- ε-Caprolactone (PCL) and Chitosan (CS), and incorporation of 5-Fluorouracil (5-FU). The aim of the first layer is releasing the drug within 4 weeks, obtaining a prolonged and modified release. According to *in vitro* drug release tests performed, ~32 % of 5-FU was released after one month, after an initial burst effect of 17.22 %. The sudden release of the drug into the body would quickly reach an effective therapeutic concentration, while the drug sustained release maintains an effective therapeutic concentration range during the administration time. The second layer is made exclusively from PCL as polymeric matrix, into which Gold Nanoparticles (AuNPs) were subsequently loaded, and its main purpose is to be radiation enhancement. The long biodegradation time of PCL would make the non-soluble scaffold an alternative to conventional chemotherapy, optimizing drug release to the specific needs of the patients.

1. Introduction

While breast cancer in men is a rare disease, occurring in less than 1 % of all the diagnosis, it is the leading cause of mortality among female population, especially for postmenopausal women (Affandi et al., 1987; Moo et al., 2018). The high heterogeneity of the tumour leads to a wide range of treatments, classified as *standard* or *clinical trials* (Akram et al., 2017; Carneiro and El-Deiry, 2020). From surgery to chemotherapy, from radiotherapy to immunotherapy, reducing the onset of significant side effects and the invasiveness of therapies are the set goals. Implantable drug delivery devices (IDDSs) are a novel drug delivery system, which aids the identification and localization of tumour tissue and consequently improves controlling the release of the therapeutic agents. As IDDSs are placed nearby the tumour mass, they avoid the involvement of the entire system and are able to reach the site of action easier, allowing the same therapeutic effect with the use of lower drug concentrations (Stewart et al., 2018).

By using a polymeric implant, the drug delivery system could optimise safety and effectiveness of therapies. The first United States Food and Drug Administration (FDA) approved implants dates back to 1983, when Norplant® (Domínguez-Robles et al., 2021), a rod shape implant loaded with Levonorgestrel was commercialized for contraceptive purposes. *In vivo* biocompatibility and stability of the implant itself should be carefully evaluated. The different and specific properties of implants such as *in vitro* and *in vivo* drug release profiles depend on their formulation (i.e. type of polymers), but also the manufacturing can play an important role (Hussain et al., 2021). Cost effectiveness must be accurately evaluated to choose the proper manufacturing technique. Compression, Solvent casting, Hot-Melt Extrusion (HME), Injection Moulding) are the most common methods of fabrication. 3DP is a promising new alternative way of manufacturing, which developed as result of better understanding the physicochemical material's properties, enabling a change in the paradigm of quality for the 3D printed dosage forms, compared to the traditional manufacturing techniques.

* Corresponding author.
E-mail address: d.lamprou@qub.ac.uk (D.A. Lamprou).

https://doi.org/10.1016/j.ijpharm.2022.122363
Received 5 September 2022; Received in revised form 28 October 2022; Accepted 29 October 2022
Available online 3 November 2022

Not only the possibility of designing pharmaceuticals on a human scale, but also the reduced resource investment made 3DP the potential tool to accelerate clinical trials. Avoiding conventional manufacturing methods will lead to money- and time-saving efficiency. For example, producing an IDDS and having it tested immediately for its effectiveness, avoids going through the entire drug development process. In order to fabricate biodegradable implantable devices for an effective breast cancer treatment, the 3D Bioprinting process (Mathew et al., 2020) was then investigated.

Since physically removing the tumour with breast surgery is an invasive procedure, whose dimensions are between 2 and 4 cm (Lovelace et al., 2019), 3DP scaffolds would be put into the cavity near the cancerous tissue, providing the local release of chemotherapeutics and preventing cancer recurrence (Kleiner et al., 2014).

Most of the drug-eluting implants found in the literature are manufactured using processes which involve organic solvents (Espinoza et al., 2020), harmful to both the environment and laboratory staff. Moreover, most of the organic solvents are toxic and not biocompatible and their removal is a tortuous succession of steps, their use could result in lack of repeatability and reproducibility. The production method proposed in this research is "greener" and environmental friendly, without the need for solvents and it is a *One-Step process* (Weaver et al., 2022).

The goal of this work is to design scaffolds made of two layers having different functions. The first is a drug-eluting polymeric layer consisting of PCL-CS loaded with -Fluorouracil (5FU) with the aim of providing drug modified release, while the second is PCL-based with the incorporation of Gold Nanoparticles (AuNPs), whose function is to act as seeds for radiation enhancement, as a second line therapeutic modality within this single platform.

To the best of our knowledge, only few studies were carried out, where PCL and Chitosan have been directly 3D printed together (Rezaei et al., 2021). Yang et al. (2022) demonstrates how CS, a natural polymer, acts as a drug release modifier due to its porous network. It has excellent gel forming properties, good compressibility and high flexibility. The latter allows better adaptation to the anatomy of the host issue without discomfort. According to Radwan-Pragłowska et al. (2019)), CS could be considered as a haemostatic agent since the positively charged amine groups are able to interact with the negatively charged surfaces of the blood cells. Despite all the advantages, pure CS scaffolds display unstable and prone-to-collapse structure, due to low ductility and poor mechanical strength. Moreover, the goal of the designed implant is to achieve a long-term drug release, and CS alone wouldn't be able to provide it. PCL is a biocompatible and biodegradable polymer that found a lot of biomedical applications in manufacturing scaffolds for tissue regeneration and drug delivery systems. It is a semicrystalline linear polyester with glass transition temperature of −60 °C that is much lower than for other polyesters. This makes the polymer rubbery in environmental and physiologic conditions. It is degraded by hydrolysis of its ester linkages in physiological conditions with even long degradation times, up to 12 months, that depend on the polymer molecular weight. Pure PCL scaffolds would be very hydrophobic and need to be combined with more hydrophilic polymers to increase cell affinity and a better incorporation of hydrophilic drugs, such as 5-FU (Hou et al., 2011). Moreover, mixing with an hydrophilic polymer such as CS, would accelerate the scaffold degradation time, which should not be longer than 6 months.

Since the scaffold has to be placed in an area subject to daily movements, the chosen materials cannot result in a stiff product, since it would cause local discomfort and irritation. The polymers combination for the first layer will need to guarantee both favourable flexibility and adaptability, being PCL an elastic material with good mechanical strength (Domínguez-Robles et al., 2021) and CS having excellent gel forming property and intrinsic antibacterial activity (Taghizadeh et al., 2022; Kean et al., 2019).

Since AuNPs have good biocompatibility and low toxicity (Kus-Liśkiewicz et al., 2021), can be incorporated into polymeric scaffolds (Sternberg et al., 2013; Luderer et al., 2013). In this work AuNPs will be loaded in the second layer, which is drug-free. It is also known that AuNPs can absorb light at specific wavelengths (Haume et al., 2016), so they can be a useful tool either as radiation enhancers or to trigger infrared laser induced heating. The infrared irradiation will ideally result in local heat generation, leading to cancer cells death (Shrestha et al., 2016).

Full physical–chemical characterization of the drug-eluting polymeric scaffold will be carried out in this work using a range of techniques including differential scanning calorimetry (DSC), thermogravimetric analysis (TGA), Fourier-transform infrared spectroscopy (FTIR), X-ray micro-computed tomography (μ-CT) and X-ray diffraction (XRD). Tensile-stress test will be performed on the designed devices to assess how the incorporation of polymers and drugs would affect the scaffold's mechanical behaviour, and the drug release will be characterized by delivering 5-FU using an *in vitro* release model, following by cytotoxicity studies.

The main goal of this research is to investigate the manufacturability of the two layers scaffold through 3DP, and it particularly focuses on the drug delivery of the chemotherapeutic agent loaded into the implant.

2. Materials & methods

2.1. Materials

Polycaprolactone powder (MW 50,000 Daltons; Tm = 58℃; PCL) was supplied by Polysciences Inc. Low molecular weight chitosan powder (Mw < 100 kDa, Deacetylation Degree ≥ 75 %; Tm = 102.5℃; CS), 5-Fluorouracil (MW 130.08 g/mol; solubility in water 12.2 g/L; Tm = 282℃ with decomposition) (Fig. 1) and tablets of phosphate-buffered saline (PBS, pH 7.4) were purchased from Sigma-Aldrich.

2.2. 3DP scaffold design and manufacture

Each scaffold was designed using Tinkercad, a free and easy-to-use computer-aided design (CAD) tool, which allows creating own 3D models adopting solid geometries. The finished designs have been saved into Standard Tessellation Language (.STL) format (Fig. 2), where information regarding geometrical location for all three dimensions are collected without considering colour and materials.

BIOX™ Bioprinter (CELLINK, Sweden) was used for the scaffolds manufacturing. BIOX™ is equipped with different printheads based on the research necessities; for the current studies, the Thermoplastic Printhead was chosen. With a heating capacity of up to 250℃, it ensures melting of thermoplastic materials. Clean Chamber Technology™, integrated by a dual high-powered fan channel air and UV-C germicidal lights, is provided in order to achieve a sterile environment for the implantable scaffolds. The device, allows removal of nearly 100 % of unwanted particles and microorganisms.

2.3. Manufacturing of scaffolds

Extrusion-based technologies are useful for the printing of high viscosity materials, such as PCL. The first scaffolds made from only PCL were fabricated following Cellink Printing Protocol, regarding temperature and applied pressure. In accordance to the BioX PCL printing protocols, the heat extrusion was set at 180℃, and the suggested pressure was 175 kPa. PCL powder was transferred into the stainless-steel cartridge without adding any solvent. PCL was melted at printing temperature, while 5-FU was still a powder at this temperature because its melting temperature is 282 °C. A 22G nozzle (0.413 mm internal diameter) was chosen for the PCL-scaffold, allowing good printability. Cannula length was 14.5 cm.

A mixture of PCL and CS was selected to carry out all the experiments. PCL is commercially available with various molecular weights; 50000 Da Mw is an intermediate molecular weight for this polymer and

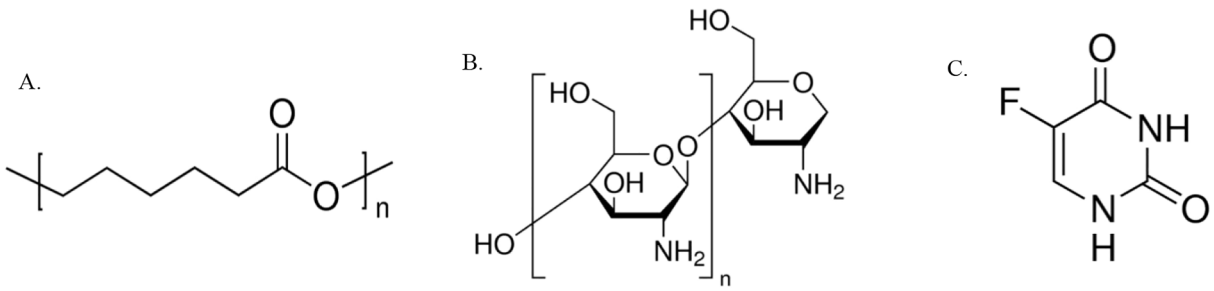

Fig. 1. Chemical structures of Polycaprolactone (A), Chitosan (B), 5- Fluorouracil (C).

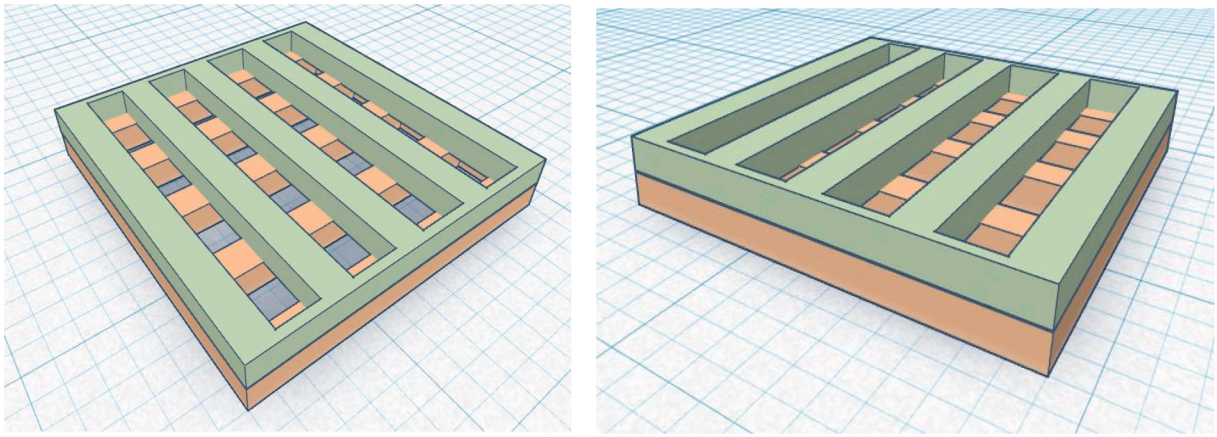

Fig. 2. CAD 3D image of the two layers scaffold before printing (l = 21.0 mm; w = 18.0 mm; h = 1.0 mm).

it was selected on the basis of the melted polymer viscosity that was suitable for 3Dprinting (data not reported). A preliminary screening was carried out to determine which polymer combination gave the best results in terms of powder flow and printability On the basis of the results (data not reported reported)30/1 PCL-CS w/w combination (3.33 % w/w CS concentration) was chosen. Since both polymers were supplied in powder forms, they were blended using vortex without adding any solvent (Glover et al., 2022). To ensure a homogenous mixture, the polymers were vortexed five times for 60 s each time prior of printing. The optimized printing parameters for the PCL-CS scaffold are different from the PCL printing protocol by Cellink, as shown in Table 1. Changing the nozzle diameter from 22G to 18G (0.838 m internal diameter) and increasing the pressure from 175 kPa to 195 kPa, allowed a better material flow. To assess good printability and to avoid deposition of any additional material, speed was increased to 3.5 mm/s. Lowering the temperature was the key to avoid PCL turning brown, which meant it was about to degrade.

2.4. Manufacturing of Drug-loaded scaffolds

The present study uses 5-FU as the drug to be loaded into the 3DP scaffolds for the treatment of cancer. The drug loading in the scaffolds was assessed as 1 % of the total weight. To ensure homogeneity of the polymers and drug mixture to be printed, the same vortexing procedure as carried out on the empty scaffolds was repeated on the polymers plus drug (5x60s).

Table 1
Bioprinting parameters used to produce (A) PCL scaffolds, (B) PCL-CS scaffolds, (C) PCL-CS-5FU scaffolds, and (D) PCL-AuNPs scaffolds.

Scaffold	Temperature (C)	Pressure (kPa)	Layer height (mm)	Speed (mm/s)	Infill density (%)
PCL	180	175	0.413	2.0	25
PCL-CS	130	195	0.838	3.5	25
PCL-CS-5FU	130	195	0.838	3.5	25
PCL-AuNPs	130	195	0.413	3.5	25

2.5. Au nanoparticles synthesis & characterisation

2.5.1. Synthesis

Gold nanoparticles were synthesised via addition of chloroauric acid (4 % $HAuCl_4$, 375 μL) into 100 mL of icy water with stirring. Subsequently. 0.2 M of sodium carbonate (Na_2CO_3, 500 μL) was added to solution and stirred for 5 min. Sodium borohydride (5 mL, $NaBH_4$, 0.5 mg mL^{-1}) was then added slowly and the solution turned from colourless into a red solution indicating colloidal gold formation. The solution in order to be use in the bioprinting formulations was freeze-dried.

2.5.2. Transmission electron microscopes (TEM)

TEM imaging was carried out using the JEOL JEM-1230 with Analysis software (JEOL, Japan) transmission electron microscope. Formvar coated copper grids were prepared, and the nanoparticles were pipetted (10 μL) onto the grids and allowed to air dry before imaging.

2.5.3. Freeze-drying of AuNPs aqueous suspension

The freeze-drying instrument (VirTis, Wizard 2.0, SP Industries Co, NY, USA) was set to −60℃, before the glass vials were put into the chamber to avoid particle's precipitation due to excessive change of temperature. The samples were placed into the chamber and the recipe was loaded from the software into the machine. The FZ temperature was firstly set at −50℃ with a vacuum of 60 0 m-Torr for 24 h, resulting in completely dry powder after first and secondary drying. The whole process was conducted without additives and/or cryoprotectants. The AuNPs powder were then mixed with the polymers used for 3DP. The

subsequent analysis relating to the particle size was carried out by TEM after freeze drying.

2.6. Scaffold characterization

2.6.1. Thermal properties

The thermal behaviours of PCL powder, CS powder, 3DP PCL, 3DP PCL-CS, 3DP PCL-CS-5FU scaffolds were analysed with a differential scanning calorimeter (DSC) 214 Polyma (NETZSCH-Gerätebau GmbH, Wolverhampton, UK). The samples were weighted in a 5–10 mg range and placed in aluminium crucibles. Starting from 25℃ (Room Temperature, RT), the powder samples and the empty scaffolds were heated up 200℃ (Yang et al., 2022), while the drug-loaded ones were heated up to 400 ℃ to highlight the nature of the drug. Scanning rate was 10 K/min, under protection of nitrogen purge gas (flow rate 40.0 mL/min). All experiments were run in triplicate to minimize the statistical error.

The thermal gravimetric analyser (TGA; Q50, TA, USA) was used to investigate the behaviour of the different scaffolds over a progressive increase of temperature. Sample weight was around 6 mg and the samples were placed in a platinum crucible. The ramp rate was set to 20 ℃/min from RT to 500℃, under protection of nitrogen purge gas (flow rate 50.0 mL/min).

2.6.2. Fourier-transform infrared spectroscopy (FTIR)

Attenuated Total Reflection-Fourier Transform Infrared Spectroscopy (ATR-FTIR) was used to analyse both powders and 3D printed scaffold to detect potential chemical interactions or chemical modifications among the materials. Each sample spectrum was obtained between 4000 cm^{-1} and 400 cm^{-1} range using a Nicolet™ iS50 FTIR Spectrometer (Thermo-Fisher Scientific). Samples were run multiple times at a resolution of 4 cm^{-1} with 64 scans after background correction.

2.6.3. Mechanical properties

Both flexibility and brittleness properties of the 3DP scaffolds (PCL; PCL-CS: PCL-CS-5FU) were evaluated through the Texture Analyzer TA. TX-Plus (Stable Micro Systems, Surrey, UK)3DP scaffold were printed in a 5 cm × 1 cm shape to best fit between the instrument's clamps, which were put at 35 mm distance. The clamps' speed was set at 5.00 mm/*sec* under a trigger force of 0.049 N, until the distance of 200 mm was reached. The Tension mode was set, allowing the Texture Analyzer to move the probe up. Triplicate measurements were performed for each scaffold formulation. The resulting graphs are reported as force (N, Y) *vs* distance (mm, X). Based on the obtained results, it was possible to graph the result as Stress (σ, Y) *vs* Strain (ε, X), using equations (1) and (2). Maximum elongation, UTS (Ultimate tensile strength) and Young Modulus were then calculated and used to characterize the different 3DP scaffolds.

$$Stress(\sigma) = \frac{Force(N)}{Crosssectionarea(mm^2)} \quad (1)$$

$$Strain\ () = \frac{Displacement\ (mm)}{Clamps'distance\ (mm)} \quad (2)$$

$$MaximumElongation = \frac{(FinalGaugeLenght - InitialGaugeLenght)}{InitialGaugeLenght} x100 \quad (3)$$

$$UTS = Maximum(Stress(\sigma)) \quad (4)$$

$$YoungModulus = \frac{Stress(\sigma)}{Strain(.)} \quad (5)$$

2.6.4. Crystal structure and morphological characterization

X-ray diffraction patterns of PCL, PCL-CS and PCL-CS-5FU scaffolds were determined using a Malvern Panalytical Empyrean-3 system (Malvern, UK), equipped with a Cu Kα source. Samples were analysed in a 5°-65° 2θ range, at increments of 0.0033°. The scan speed was set to 0.018°/*sec* in a continuous scan mode. Results were then evaluated via the Data Collector software.

Scaffolds' morphology incorporated with AuNPs were evaluated through X-ray microcomputed tomography (μCT). The analysis were performed placing the 10x10 mm samples inside a dental wax, and a Bruker Skyscan 1275 with Hamamatsu L11871 source at 45 kV and 30uA was used to collect the 2D images. The resulting images were 900x152 pixels with a resolution of 16.10 μm per pixel. The total exposure time was 100 ms with a rotation step of 0.2°, averaging three frames for each 360°rotation. The 3D reconstruction was performed manually via BrukerCTvol software and the attenuation thresholding was carried out to remove spots around the sample.

2.6.5. Optical microscope

The morphological analysis was performed with a stereo microscope integrated by a camera (Leica EZ4W, Leica Microsystems, Milton Keynes, UK). The observations were focused on AuNPs' incorporation into the 3DP scaffolds. After freeze-drying, the AuNPs' were clearly visible as black spots both on the surface and inside the implant.

2.6.6. Drug content determination and in vitro drug release test

5-FU was analysed by UV spectrophotometer both for determination of the amount of drug loaded into the scaffolds and *in vitro* released. The spectrum was recorded in triplicate with a 7205 Jenway UV–vis scanning UV-spectrophotometer (Cole-Parmer, Staffordshire, UK), and the absorbance at a wavelength of 266 nm was measured (Ortiz et al., 2012). The actual amount of 5-FU loaded in the scaffolds was determined as follows. The whole scaffold (about 42 mg) was dissolved in 5 mL of chloroform and then purified water was added for extracting 5-FU. The system was maintained under magnetic stirring at 1000 rpm for 1 h to promote 5-FU extraction. The chloroform/water mixture was centrifuged (Domínguez-Robles et al., 2021) in order to separate organic and aqueous phases. 5-FU was recovered in the aqueous phase and its amount determined by spectrophotometric analysis. The amount of actual drug loaded was determined in triplicate on 3 scaffolds manufactured with the same batch of polymer/drug mixture, according to the following equation (6). The extraction protocol was validated and extraction yield was confirmed to be 95 ± 3.0 %.

$$Drugloading(\%) = \frac{Actualamount5-FUinonescaffold(mg)}{Totalweightofscaffold(mg)} \times 100 \quad (6)$$

5-FU loaded scaffolds were tested to determine the *in vitro* drug release. Same set up of *in vitro* release test was used, as described by Corduas et al. (2021), with slight modifications. Throughout the experiments, PCL-CS (control) and PCL-CS-5FU scaffolds were stored in glass vials containing 4 mL of PBS each in an incubator at constant temperature of 37 ± 0.5 °C. Before starting the experiments, accurate weighting of each scaffold was carried on in order to evaluate the weight loss over time. The experimental time-points were set at 2 h, 4 h, 24 h, 48 h, 72 h and then once a week until a plateau was reached. For every sampling, 1 mL of medium was withdrawn from the samples and replaced by fresh one. Each sample was analysed by UV-spectrophotometer (Cole-Parmer, Staffordshire, UK) at a wavelength of 266 nm and absorbance was measured (Ortiz et al., 2012).

The percentage of drug released at each time point was calculated according to equation 7.

$$Drugreleased(\%) = \frac{Amountofdrugreleasedattimet(\mu g)}{Actualamount5-FUinonescaffold(\mu g)} \times 100$$

2.7. In vitro biocompatibility study

Human epithelial breast cancer (MCF-7) cells in exponential growth

phase were seeded into 6-well flat-bottomed plates and incubated for 24 h at 37 °C with 5 % CO_2. The media were replaced with 2 mL fresh media and the scaffolds (PCL, PCL-CS, PCL-CS-5FU, PCL-AuNP) were placed in the wells and incubated with the cells for 24 h, subsequently the media were removed, and the cells were washed 3 times with PBS. The cells were trypsinied and re-suspended in fresh media. A mixture of 50 μL of cells and 50 μL of trypan blue solution was placed in an automated cell counter (Invitrogen Countess®, UK) and viable cells were counted. Percentage cell viability was calculated and expressed as a percentage in relation to the number of control cells (incubated without scaffold).

2.8. Statistical analysis

A statistical independent sample *t*-test (parametric test) was used to compare means of two independent groups within the Microsoft Excel software package, where significance was deemed at $p < 0.05$.

3. Results & discussion

3.1. Materials selection

PCL and CS were the chosen materials providing a biologically and mechanically suitable 3D printed drug-eluting polymeric scaffold for an effective breast cancer treatment. PCL is a distinguished material, commonly used in Additive Manufacturing (AM) for biomedical applications due to its biodegradability, biocompatibility and remarkable mechanical properties. PCL, as a biomaterial, shows great processability, and the 3DP scaffolds made of PCL display high surface area and high permeability (Corduas et al., 2021). Due to its semi-crystalline nature, it degrades at a slower rate if compared to other biocompatible polymers such as Polylactide-*co*-glycolide (PLGA, 50/50 monomer ratio), that is due to degrade in between 30 and 45 days, depending on its molecular weight. PCL degradation time increases with its molecular weight, and 50KDa PCL was chosen in order to shorten its biodegradation time, since the drug-eluting layer of the scaffold is expected to release the drug during one month, according to the formulation study.

Despite PCL being suitable for controlled and sustained drug release, the polymer is very hydrophobic. One of the reasons that PCL was chosen to be combined with CS, a natural and biocompatible material, is that if PCL were used alone would have had low bioactivity and low surface energy. Being CS derived from deacetylation (DD) of chitin, each monomer has a free amine group and the polymer possesses good hydrophilicity but pure CS scaffolds display unstable and prone-to-collapse structure due to its low ductility and poor mechanical strength. Since 5FU, is hydrophilic and CS has excellent gel forming properties and an open porous structure, the drug chosen can easily dissolve in the swollen CS. CS is extensively employed as biomaterial because of its wide variability in molecular weight (MW) and DD. MW and DD are the most important parameters influencing CS' *in vivo* properties and behaviour. Low molecular weight CS with a lower degree of acetylation was chosen. According to Younes et al. (2014), it has both a higher antibacterial activity at pH 7.4 and it is more active in scavenging free radicals. From a manufacturing point of view, it has low viscosity and could be extruded from the cartridge easily, resulting in good compressibility. Moreover, its high flexibility will lead to a better adaptation to the anatomy of the host tissue. CS degradation kinetics and the resulting weight loss are controlled by the DD. While higher DD% showed very slow degradation process, decreasing the MW and the DD lead to faster degradation, as pointed out by Ren et al. (2005). Combining a fast degradable biopolymer, as CS with PCL, known for having long biodegradation time, was the key reason why these materials were chosen to carry out the set goal.

PCL alone is being used as coating polymer to slow down the drug release from long-acting delivery systems. Once the dissolved drug permeates through the scaffold, it can be released into the medium, prolonging the release (Stewart et al., 2020). Since the high hydrophobicity of PCL alone would lead to low affinity with the drug incorporated into the printed scaffold, low MW CS was chosen to speed up the drug release from the implant, trying to obtain a drug therapeutic concentration in a shorter period of time.

5FU, a derivative of uracil, is one of the oldest but still effective cytotoxic drugs for breast cancer treatment, frequently used in single modality for solid tumours. It acts as a competitive inhibitor of deoxythymidylate acid, as it binds to thymidylate synthetase (TS), irreversibly blocking it. Since it interferes with nucleotide synthesis and incorporates into DNA, has mutational impact on surviving tumour cells but also on healthy ones. To overcome the problem of poor selectivity due to systemic involvement, the chosen drug was incorporated into the polymeric scaffolds, to achieve localized targeting and controlled drug delivery. It has also been suggested that the incorporation of CS may prevent side effects related to 5FU administration (Kimura and Okuda, 1999), due to the selective inhibition of the drug uptake into the small intestine and spleen. Since the polymeric scaffold is meant to provide both improved bioavailability and targeted drug delivery being placed nearby the cancerous tissue, less chemotherapeutic agent is needed with respect to a systemic administration. The drug was homogeneously dispersed within the polymers, and loaded into the cartridge in a 1 % w/w concentration. The drug loading also resulted in 5-FU acting as a filler during the pressure-assisted extrusion without the need of it being completely melted, allowing better printability.

The second layer is drug-free and consisted of AuNPs (TEM shown in **Figure SI 1**), homogeneously dispersed within PCL, which observed by microscopic analysis. Since PCL has already been used alone, trying to achieve long biodegradation time, the rationale of the study was to formulate and manufacture a scaffold which could be implanted in the body for at least one year, in order to make the most of the radiation therapy when needed, if cancer recurrence occurs. AuNPs were incorporated into the biodegradable scaffolds to make the most of a long-acting therapy, such as radiotherapy, which exploits the specific wavelength of the NPs to selectively target the tumour tissue. It is also known that AuNPs can result in local heat generation, ideally achieving both phototherapy and radiotherapy.

3.2. Scaffold design and printing

CellInk BioX was used to prepare the scaffolds in a *One-Step Process*. After a homogeneity of the powders was obtained by vortexing, the materials were directly put into the cartridge. The scaffold printability was optimized according to Table 1, reaching a compromise between printing quality and printing time. Printing temperature was decreased from 180℃ to 130℃, avoiding PCL turning brown due to its denaturation. Despite PCL has a lower melting temperature (Tm = 58℃), a higher temperature had to be used since the Thermoplastic Printhead heats the cartridge from outside.

The infill density stayed stable at 25 %, allowing both the printing of pore-free scaffolds, which could have led to the premature release of the drug otherwise, and a lower printing time. Nozzle diameter and layer height increased from the 22G nozzle (0.413 mm internal diameter) to the 18G nozzle (0.838 mm internal diameter). The addition of CS to PCL scaffolds and the simultaneous use of a temperature lower than CS melting point, have influenced this choice, resulting in chitosan acting as a filler in the polymer processing. To prevent both the deposition of too much material, due to the nozzle diameter, and the pressure increasing up to 195 KPa, which could have resulted in poor quality printing, printing speed was set to 3.5 mm/s. A balance between the printing parameters and the loaded materials' blend composition into the cartridge was obtained with minor difference between the designed scaffold and the result achieved after printing. Fig. 3 shows representation of the 3D printed first layer scaffold design loaded into the BioX software (on the left) and printed scaffold result (on the right), with their respective measurements. The scaffolds were measured in triplicate and the differences between theoretical, and actual scaffold measures are

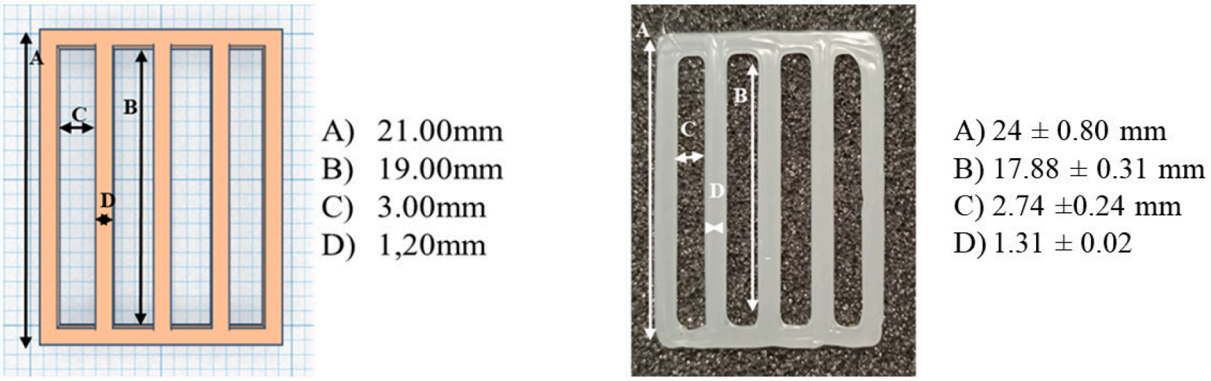

Fig. 3. Representation of the 3D printed first layer scaffold design loaded into the BioX software (on the left) and printed scaffold result (on the right), with their respective measurements.

due to polymer relaxation after printed.

3.3. Scaffold's thermal behaviour

The scaffold's thermal stability was assessed through DSC and TGA analysis, in order to understand if and how the temperatures used in the manufacturing process influenced the materials' behaviour. Analyses were first performed on pristine powders of the materials being used, and subsequently on the printed scaffolds. The DSC thermograms of PCL powder is shown in Fig. 4**A**. The onset temperature is 51.6℃, while the endothermic peak displayed at around 62℃ corresponds to PCL Tm. Being PCL a thermoplastic material the relatively low melting temperature indicates good processability so that the optimized printing conditions do not require high temperatures, which mayresults in incompatibilities with the active ingredient. Low molecular weight CS has a broad endothermic peak around 170℃ (Tm) with an onset temperature of 141.4℃. CS is a natural polymer, which is very hygroscopic in nature and the peak shown in Fig. 4**B** is due to the water evaporation during the DSC analysis.

The temperatures being used in the 3DP process are lower than its Tm, resulting in CS acting as a filler in the manufacturing of the scaffold. The chosen drug has a good thermal stability up to its melting point (results not shown). 5FU onset temperature is about 274.5℃ and the Tm is 280.1℃, displayed through a sharp endothermic peak, which is the highest temperature that can be reached before its degradation. The influence of CS and 5FU on PCL thermal stability was monitored by comparing the 3DP scaffold's thermogram. Fig. 5B shows the DSC curve of the 3DP drug-free PCL-CS scaffold, where CS was loaded in a 1/30 w/w concentration, as mentioned before. It was not possible to detect the CS endothermic peak because of both the low amount of polymer added compared to PCL and the changing in the materials' crystalline state during the manufacturing process. The same analysis was repeated with the drug-loaded scaffold, as shown in Fig. 5**B**. Once again, due to the Limit of Detection (LOD) of the instrument and to the very low drug concentration, the 5FU peak on the DSC curve is not displayed. However, PCL Tm peak shifted to 65 °C in drug loaded scaffolds.

After the scaffold's first layer characterization, DSC analysis was performed on the second layer containing the gold NPs. While the polymer peak stayed stable with a slight difference of 0.4℃ related to the onset melting temperature and the same endothermic peak, DSC curve of the PCL-AuNPs layer revealed an exothermic peak at around 255-265℃ (**Figure SI 2**).

Both the layers underwent TGA analysis, to understand clearly the materials' behaviour inside the cartridge during the 3D Printing Process. The test was performed up to 500 ℃ to verify the PCL's complete degradation, and how incorporating polymer, drug and NPs affected its stability. The results show that under the highest manufacturing temperature, 180℃, PCL did not lose any weight. It has an excellent thermal stability up to about 400℃, a temperature much higher than the printing one. Mixing PCL with CS and 5FU did not significantly modified the polymer's thermal behaviour and its weight loss started at around the same onset temperature (Fig. 6**A**).

Based on the graph's results, the 3DP process could be assessed as safe since no loss of material occurred at the printing temperatures. Therefore, it is not possible to find any waste material inside the cartridge, which could affect the biocompatibility and the safety of the entire process.

While adding the polymer and the drug did not result in any change in the PCL's TGA curve, the incorporation of 0.25 % w/w concentration of AuNPs led to an increase in thermal stability (Fig. 6**b**).

The results obtained from TGA analysis show a difference in both temperatures, T_{Onset} and T_D, where T_{Onset} is the first temperature where the weight loss occurs and T_D is the temperature of maximum degradation rate. T_{Onset} increased from 262 ℃ to 283 ℃ by adding the AuNPs into the PCL layer. The differences are due to incorporation of AuNPs in the second layer, which appears to have a stabilizing effect on the polymeric layer made from PCL.

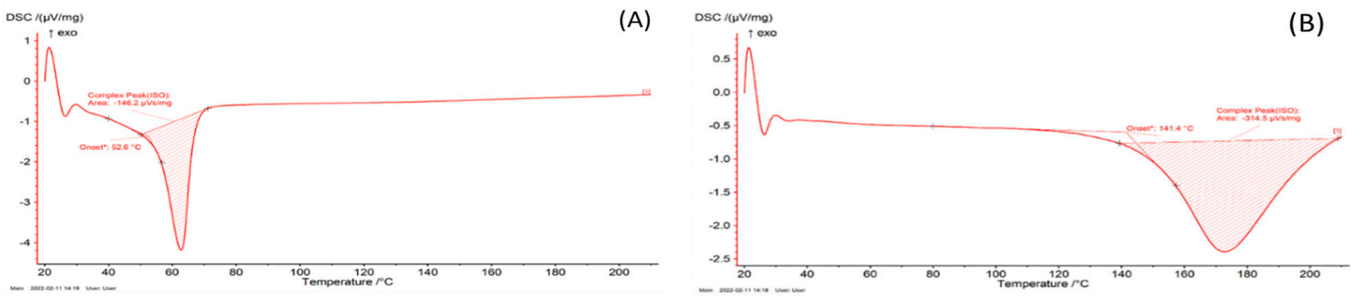

Fig. 4. DSC heating curves of PCL powder (A) and CS powder (B).

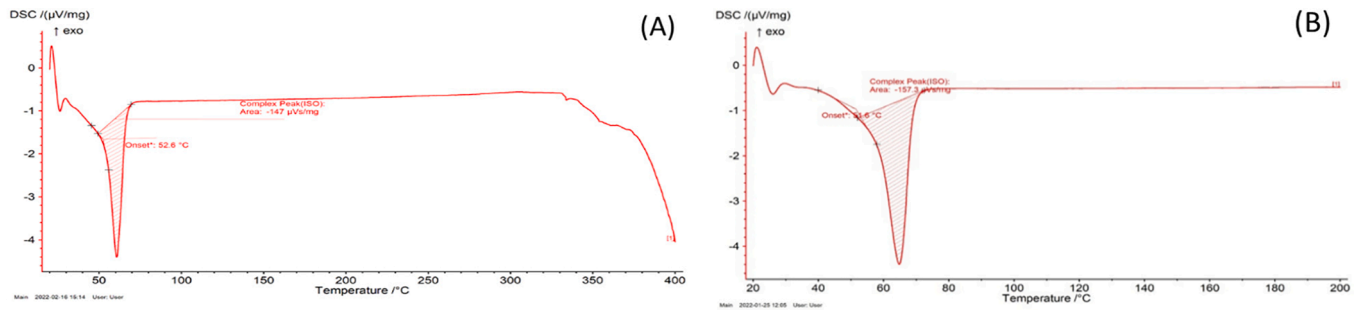

Fig. 5. DSC heating curves of the 3DP drug-free scaffold made of PCL-CS (A) and the 3DP drug-loaded scaffold made of PCL-CS-5FU (B).

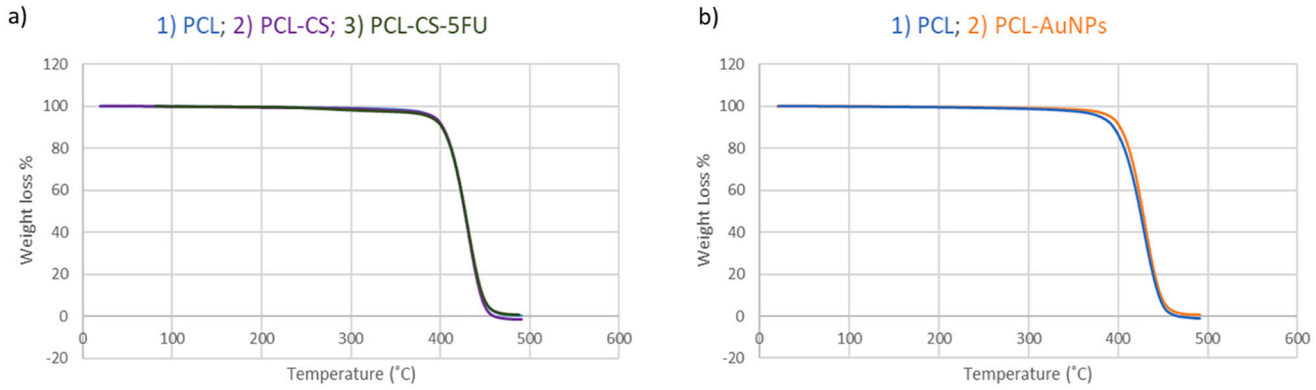

Fig. 6. TGA analysis of: a) 1)3DP PCL scaffold, 2) 3DP PCL-CS drug-free scaffold and 3)3DP scaffold PCL-CS-5FU drug loaded scaffold; b) 1) 3DP PCL scaffold and 2) 3DP PCL-AuNPs scaffold.

3.4. Spectroscopic analysis

FTIR analysis were conducted on the 3D printed scaffolds to evaluate how the manufacturing process affected the chemical interactions between the materials. Their FTIR spectra are reported in Fig. 7 and compared with FTIR spectra (**Figure SI3**) of pristine materials before printing.

CS content cannot be detected in the spectrum of either PCL/CS or PCL/CS/5FU scaffolds (Fig. 7 green line and red line) because of its low content. Therefore no changes in the spectrum are registered by adding CS to PCL if compared to the FTIR trace of PCL pristine material (see **Figure SI3B**), while incorporation of 5-FU determines changes in FTIR spectrum of PCL/CS/5FU. The 3DP drug loaded scaffold shows the two typical peaks at around 3200 cm^{-1} (A circle in Fig. 7) and at 1640 cm^{-1}

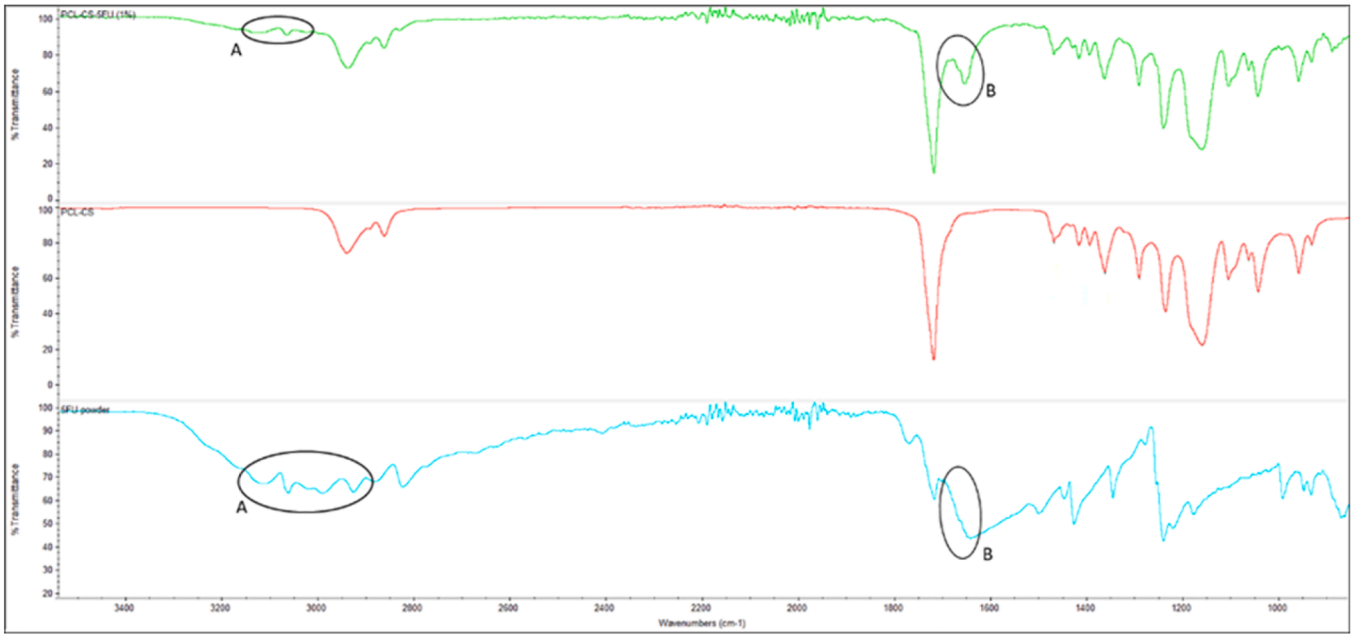

Fig. 7. FTIR spectra comparing the 3DP drug-loaded scaffold and the 3DP drug-free scaffold. Green line: PCL/CS/5FU (1%) scaffolds; red line PCL/CS scaffold; light blue line 5FU powder. (For interpretation of the references to colour in this figure legend, the reader is referred to the web version of this article.)

(B circle in Fig. 7) related to 5FU and the peaks' position in the two traces (blue line and green line)fall at almost the same wavelengths. Their intensity is instead reduced due to the small amount of material loaded into the scaffold, which is 0.5 % w/w of the total weight. The spectrum displays the characteristic peaks without excessive wavelength shifting, demonstrating that no chemical bonds were formed between the drug and the polymers in the scaffold during the 3DP process.

The same analysis was then performed for the second layer to investigate how the AuNPs would affect the PCL chemical bonds. The number of nanoparticles incorporated into the scaffold (0.25 % w/w concentration) was too low to detect any peaks or wavelength's shifting from the PCL scaffold. As can be seen from **Figure SI 4**, the same spectrum was obtained without any differences.

3.5. Structural characterization

In order to study the effect of the polymer and the drug on the PCL's internal crystal structure, XRD analysis were performed on the scaffold first layer's materials (Fig. 8). The first spectrum regarding the PCL scaffold shows two sharp peaks at $2\theta = 21.38°$ and 23.67°, which are assigned to (1 1 0) and (2 0 0) diffraction planes respectively. Another relatively weak peak is displayed at $2\theta = 15.70°$. The closeness of these two peaks demonstrates the crystalline nature of PCL, while the relatively weak peak at $2\theta = 15.70°$ is indicative of the polymer's amorphous regions. These three peaks are characteristic of PCL and indicate for its semi-crystalline nature.

The same analysis was then performed after CS addition to better understand how the internal structure of polymer changes during the 3DP process. While the typical CS peaks are not shown due to its low concentration, the typical peaks of PCL showed an important reduction in intensity. Their intensity decreases from Max (PCL) = 17750 cps to Max (PCL-CS) = 9397 cps. This reduction in intensity indicates that the PCL-CS scaffolds have an amorphous structure due to a decrease in crystallinity. The changing in the materials' crystalline state due to manufacturing process justifies the absence of chitosan peak within the DSC graph, as previously assumed by Yang et Al. (Yang et al., 2022). At the same time, this phenomenon also confirms the good miscibility of the different materials in the PCL-CS blend. The third analysis regards the incorporation of the drug into the 3DP scaffold. The 5-FU characteristic peaks are shown at $2\theta = 29.30°$ and 29.71°, and are due to its high crystalline nature. An increase in the PCL peaks' intensity can be clearly seen from the XRD spectrum. The Max (PCL-CS-5FU) = 16353 cps demonstrates how adding a highly crystalline material into the mixture helps preventing its phase-change into the amorphous state.

The two different diffraction patterns of phase-change relied on the molecules inserted into the PCL macromolecular chains, which resulted in different effects on its internal structure. If addition of a typically amorphous polymer such as CS caused a reduction in the material's crystallinity and weakened the intermolecular forces of PCL, on the contrary, adding a very crystalline drug as 5FU restored the high crystallinity of the mixture.

The AuNPs distribution within the printed layer of PCL was investigated by 3D reconstruction of the sample, and by using Bruker CtVol software. Thanks to the difference in densities between PCL and gold (1.1145 g/cm^3 and 19.3 g/cm^3 respectively) (Corduas et al., 2021), AuNPs were clearly highlighted via thresholding process.

As shown in Fig. 9 (A-C), melt-extrusion 3D printing can be considered a successful method to encapsulate active agents inside a polymeric scaffold. Although limited aggregation phenomena can be observed due to the nature and to the reduced size of the nanoparticles, the μCT analysis shows how the AuNPs in solid form, after the freeze-drying process, were distributed within the PCL-based polymeric matrix. Similar results were also obtained using fused deposition modelling in combination with drugs (Mathew et al., 2019) and melt-extrusion 3D printing in combination with ceramics and piezoelectric particles (Mancuso et al., 2021). Giving the importance, in terms of treatment success, of achieving a uniform arrangement of active ingredients in the scaffold, the as-produced samples possess the potential to induce homogeneously a localized hypothermic effect on the cancerous cells surface and causing their death (Vines et al., 2019).

3.6. Mechanical properties

Regarding the mechanical properties of the 3DP scaffolds, in this preliminary work tensile stress test was performed to assess how polymers and drug would affect PCL's behaviour. The scaffold size was adapted for the experiments to get a better grip between the clamps, as can be seen from Fig. 10. The mechanical tests were performed according to the role that the scaffolds would play *in vivo*. The materials have been chosen so that the scaffolds will provide sufficient stability to the host tissue without causing any discomfort or pain.

From the obtained results where the force (N, Y) was plotted against the distance (mm, X), it was possible to graph the result as Stress (σ, Y) *vs* Strain (ε, X), as they are displayed in Fig. 11. To compare the different 3DP scaffolds, Maximum Elongation-UTS-Elastic Modulus were calculated and reported in Table 2 to obtain a synoptic comparison between the implants made of different materials.

The flexibility of the 3DP polymeric scaffolds was evaluated taking as a reference the implant based on only PCL. Elastic modulus relative to PCL scaffolds is the highest compared to all those proposed here, and is

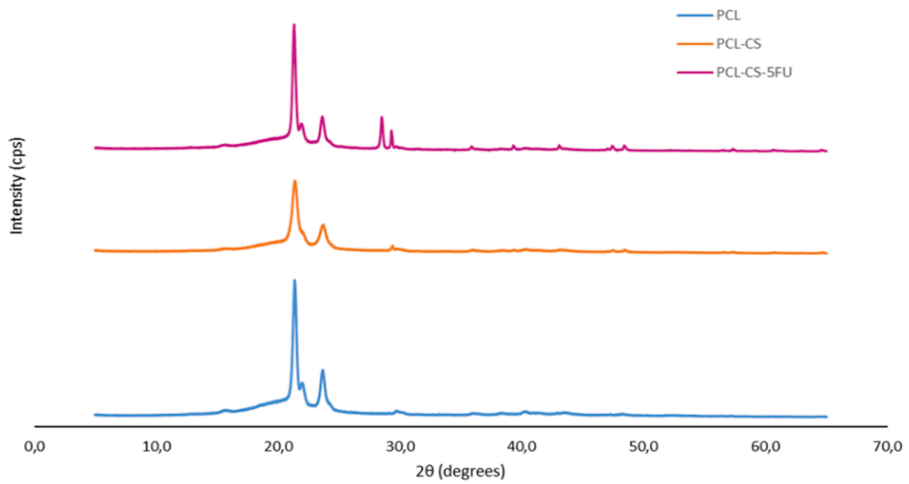

Fig. 8. XRD analysis of 3DP scaffold made of PCL, PCL-CS and PCL-CS-5FU.

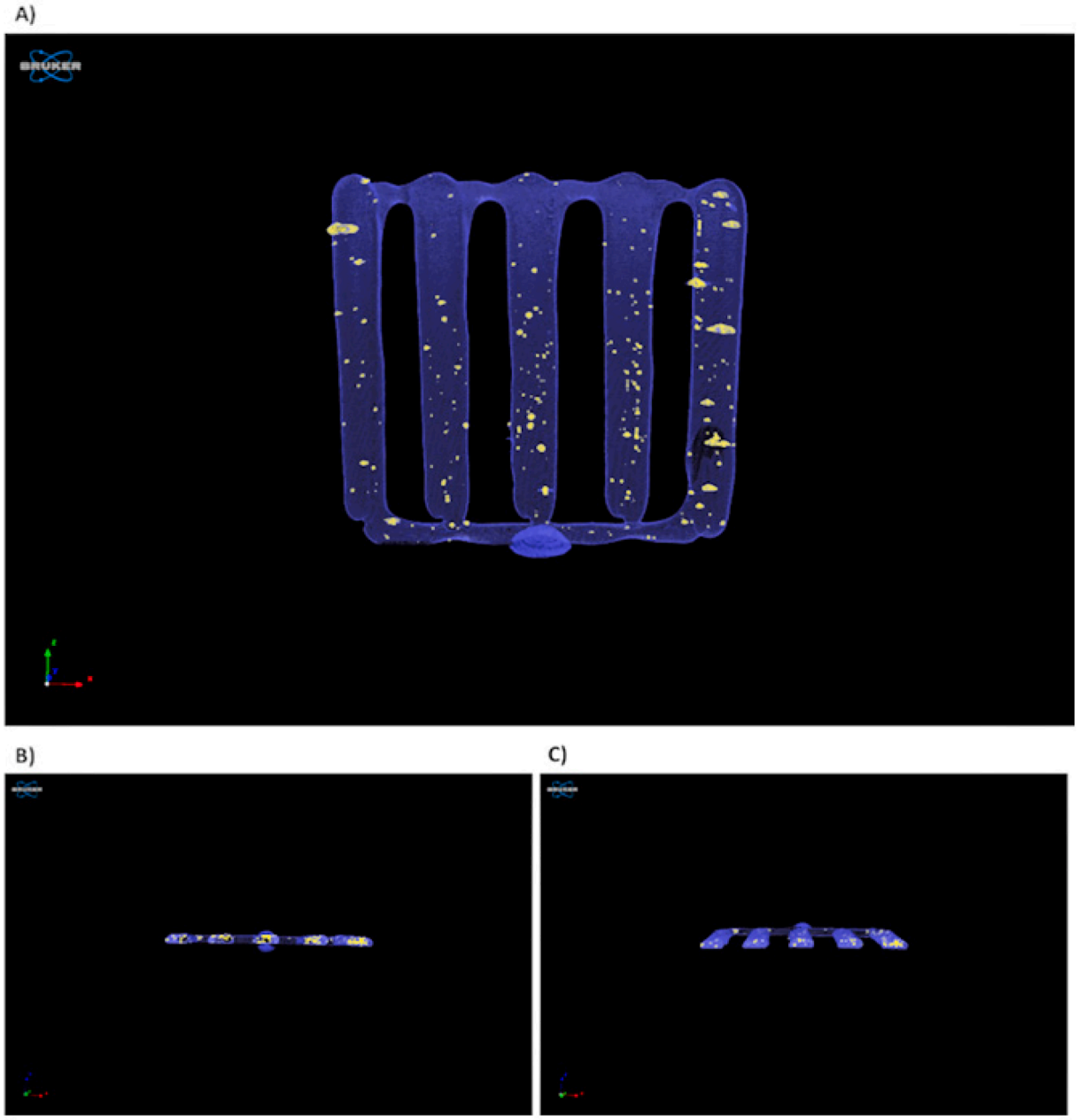

Fig. 9. X-ray microcomputed tomography reconstruction (3D slices) of the printed implant. A) Front view; B) Inferior view; C) Superior view.

equal to 18.056 ± 0.411 MPa. The force required to obtain its stretching is maximum, meaning that the material is resistant but at the same time, it does not have sufficient elasticity in the longitudinal direction. Its high resistance to the pulling between the clamps meant that at the maximum elongation of the material the scaffold was irreversibly deformed, but the break point was never reached, as can be seen in **Figure SI 5**, where the curve begins its descent phase. Given the problems related to a possible *in vivo* utilization of the scaffold made of PCL, CS has been added, being CS well known for its open porous structure, in order to make the implant more suitable for the purpose for which it was designed. The PCL-CS scaffold, as expected from the initial formulation study, showed lower Young modulus with respect to the PCL scaffolds.

The incorporation of CS into the 3DP scaffolds resulted in an 11.46 % reduction as regards the Young's modulus, which is equal to 15.986 MPa. The Young's Modulus is the slope of the initial straight line of the stress–strain curve, and the greater the slope, the more the polymeric scaffold does not deform due to significant stresses, meaning that it is rigid and resistant. The addition of CS (1/30 w/w concentration) lowered the slope, meaning that the PCL-CS scaffold is more deformable. It is also possible to find a match to this in the Maximum Elongation parameter, by observing how it goes from 0.949 %±0.057 of only-PCL to 1.104 %±0.116 of PCL-CS scaffolds. The UTS, which is the maximum stress value that the scaffold can withstand before breaking down, decreased by 6.16 % from 10.375 ± 0.413 MPa to 9.736 ± 0.715 MPa.

5FU was added afterwards and its impact on the mechanical behaviour of the scaffolds was evaluated. Table 2 shows that Young's Modulus assumes greater values when the drug is present in the formulation, if compared to the PCL-CS scaffolds. It increased to 17.521 ± 1.210 MPa (+9.60 %) recovering a slope comparable to PCL scaffolds. Maximum Elongation appears to be the lowest with a 0.863 %±0.044 value, meaning that the length that the scaffold can reach before its break point is lower than the others are. This may be due to the presence of the 5FU, which was added during the 3DP process blended with the other polymers as powder, but the process temperatures were not high

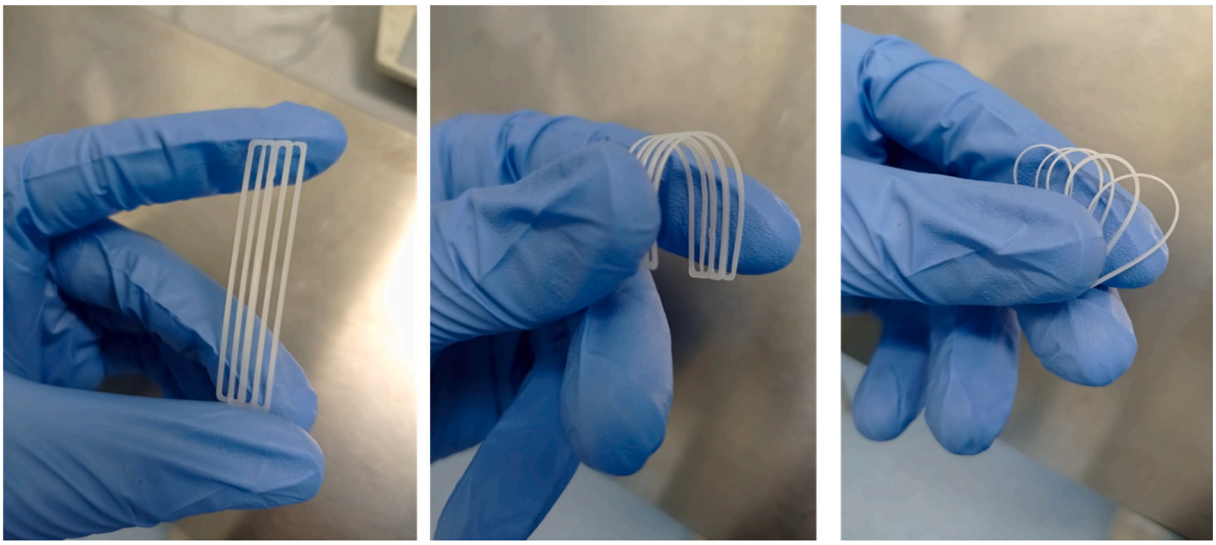

Fig. 10. 3DP scaffolds before the Tensile stress test (l = 50.0 mm; w = 10.0 mm; h = 1.0 mm).

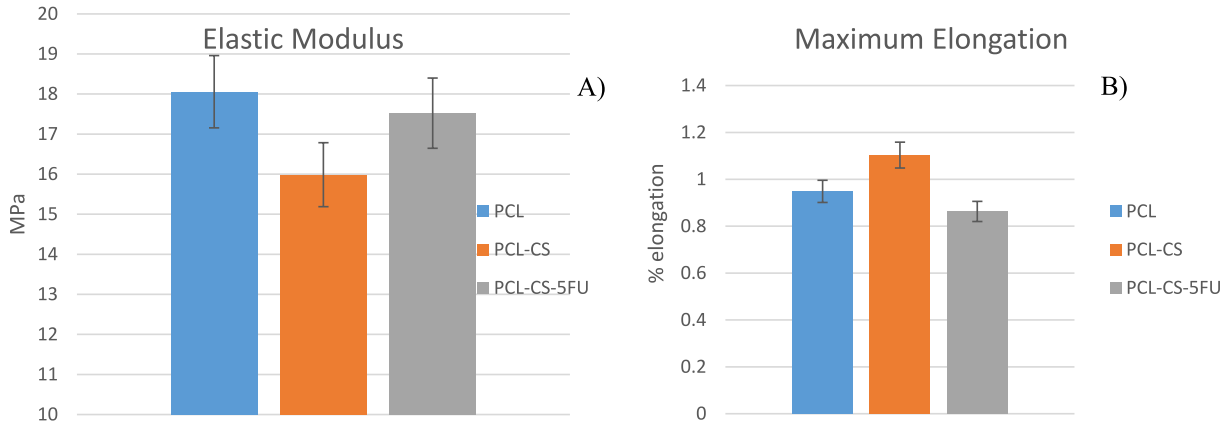

Fig. 11. A) Elastic modulus and B) maximum elongation at break of the three different 3DP scaffolds.

Table 2
Mechanical response of the 3DP scaffolds.

Sample	ELASTIC MODULUS (MPa)	MAX ELONGATION (%)	UTS (MPa)
PCL	18.056 ± 0.411	0.949 ± 0.057	10.375 ± 0.413
PCL-CS	15.986 ± 1.092	1.104 ± 0.116	9.736 ± 0.715
PCL-CS-5FU	17.521 ± 1.210	0.863 ± 0.044	10.055 ± 0.322

enough to allow it to be completely melted. Therefore, the drug was acting as a filler within the polymer blend and its presence at a microscopic level could have led to a reduction in elasticity. The PCL-CS-5FU scaffold's mechanical properties are however balanced by a UTS value of 10.055 ± 0.322, intermediate between only-PCL and PCL-CS scaffolds. The mechanical tests demonstrated how resistance to the scaffold's deformation, and therefore their Young's modulus, are strongly influenced by the composition of the matrix, the starting materials and the structural characteristics.

Interestingly, it was highlighted that even when maximum elongation strength was reached, no complete rupture occurs in the three types of scaffolds, but only intermittent failures of the singles strands that make up the implant. This feature guarantees good resistance to stretching, identifying the final scaffold as not easily breakable, and therefore suitable for providing sufficient stability to the host tissue.

3.7. Drug content determination and in vitro drug release test

Implants weight was 42.4 ± 0.692 mg as determined on the 3 implants manufactured with one batch of polymers/drug blend. Actual drug content was determined in each implant and was 0.95 ± 0.02 %, corresponding to about 95 % of the starting amount of 5-FU (1 % of powder mixture weight). *In vitro* drug release tests give a preliminary view of release behaviour of encapsulated drug. Fig. 12 shows the results as cumulative release of 5-FU, based on both the weight and percentage.

PCL is a well-known polymer for slowing and prolonging the drug release (Stewart et al., 2020), while CS has been shown to slow the release in the short term only. Choosing to combine the two polymers also derives from the attempt to speed up the release through the incorporation of CS, but at the same time retain the excellent characteristics of biocompatibility and slow-degradation time of PCL. The results obtained from the release studies confirm the hypothesis. In a total of 4 weeks, the release of 5FU was equal to 0.1348 ± 0.0025 mg, corresponding to 34.08 ± 0.6001 %.

Simultaneously, during each time-point over the drug release studies, the scaffolds were weighed to understand how their degradation occurred over time (**Figure SI 6**). Since the largest percentage of the scaffolds is made of PCL, its degradation is very slow, contributing to the long-term drug release. At the end of the studies, the scaffold weight

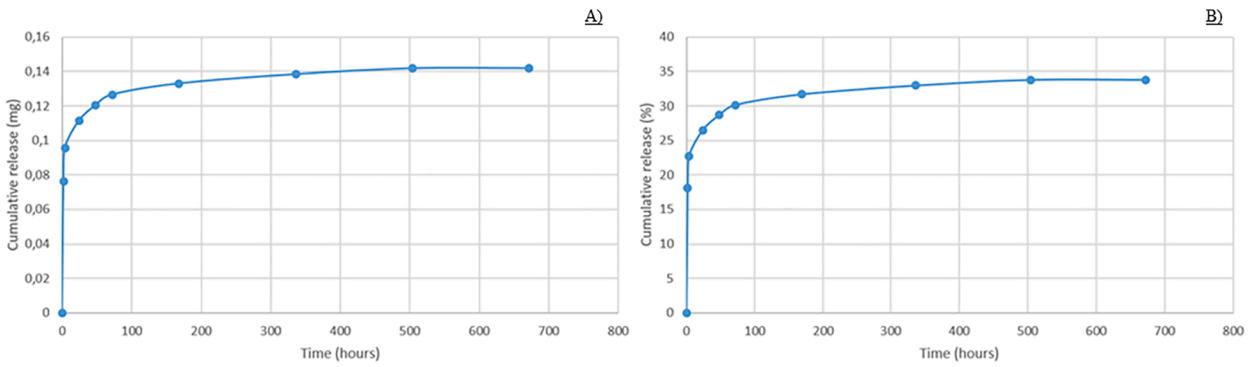

Fig. 12. Drug release profile of 5FU eluting from 3DP polymeric implants made of PCL-CS expressed as: A) cumulative mg released, B) cumulative % released.

decreased by 2.99 %, which is equal to a 1.2667 mg weight loss of material.

3.8. Gold Nanoparticles' incorporation and characterization

The second layer is drug-free and consisted in AuNPs, homogeneously dispersed within polymeric material. The mixed powders were loaded into the cartridge and printed without any additional steps, but only using the printing parameters previously optimized for the printing process (Table 1, C). As shown in Fig. 13 AuNPs were printed inside the scaffold and clearly visible through a morphological analysis with an optical microscope (Leica EZ4W), both before and after the printing.

3.9. Biocompatibility evaluation of the scaffolds

Cell viability after 24 h incubation of the samples with MCF-7 cells was measured using trypan blue exclusion. The amount of drug released after 24 h was 25.17 %, and the data shown in Fig. 14 indicate that the scaffolds were non-toxic to cells over this time period, showing good cytocompatibility. This was, with exception of the PCL-CS-5FU sample, which did result in a significant reduction in viability compared to the control cells. This finding supports the release data, showing that the highly potent 5FU is capable of permeation out of the scaffold structure, in order to carry out its function as an anticancer agent.

4. Conclusions

Customised 3DP drug-eluting polymeric implants were designed and printed with a process as environmentally sustainable as possible, without adding any organic solvent. The scaffolds are made of two layers, printed directly on top of each other. After the cooling and solidification of the first one, the thermoplastic material extruding from the nozzle at a high temperature acted as adhesive factor, consolidating the two layers, having different functions. First is a drug-eluting layer with a time-modified release of 5FU, while the second one is based on incorporation of gold nanoparticles, whose function is performed only after the radiation therapy. The synergistic approach proposed here for breast cancer treatment guarantees an alternative to conventional treatment methods that are limited to the release of chemotherapy or radiation beams that may not effectively penetrate the cancerous tissue and consequently, not eradicate the entire tumour population, making therapy ineffective with a high chance of recurrence. The 3DP polymeric scaffolds proposed in this study represent a preliminary study for a drug delivery system addressed to localized therapy of breast cancer. One advantage of the proposed localized administration of 5-FU will be a decrease of its side effects, another advantage will be the drug sustained release that permit to decrease administration frequency and increase patient compliance. After the scaffolds are implanted through surgery, they will remain stable to perform their function without further stress for the patient, being PCL well known for its long biodegradation time. These advantages will overcome the discomfort of device implantation process. The preliminary mechanical tests demonstrated scaffolds showed good mechanical behaviour and the sustained drug release, in the tested time, happened without relevant mass loss, meaning that the polymers' biodegradation will occur in a longer period of time. As long as mechanical properties are concerned, they will be verified in further studies after simulated use conditions, and if these properties remain over time (storage stability study). This preliminary study was addressed to implant formulation study and 3D printing parameters set up. After having optimized the printing parameters to avoid that the materials

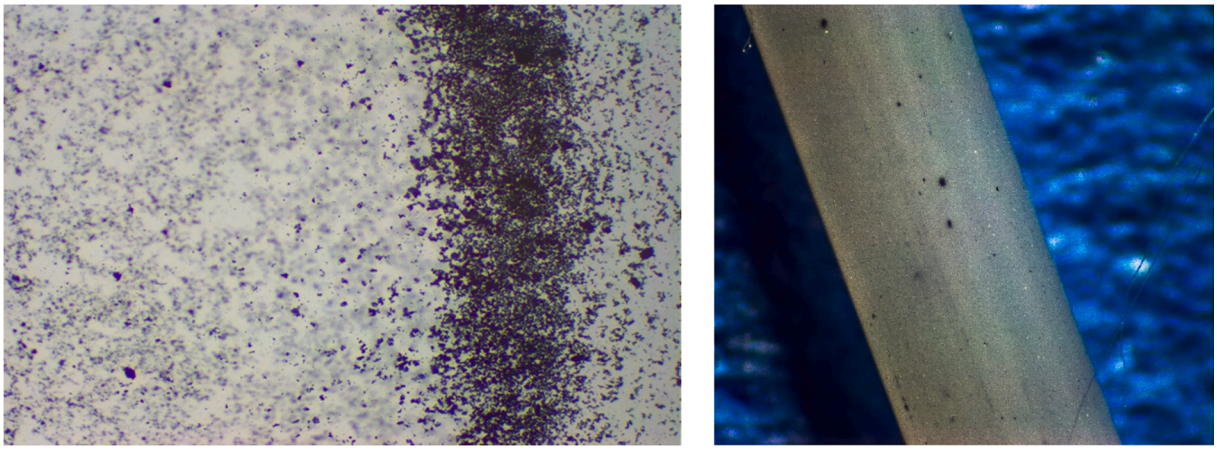

Fig. 13. AuNPs in the aqueous solution before the printing process (left; image was taken after rinsing the freeze-dried AuNPs with water) and AuNPs in the 3DP scaffold after the printing process (right), as they appear as black spots into the PCL matrix (350 × magnification).

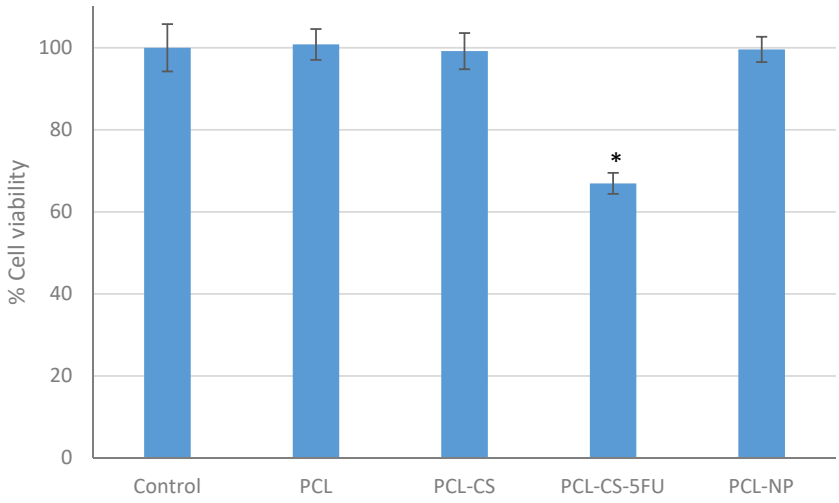

Fig. 14. Cell viability of scaffolds incubated with MCF-7 cells for 24 h, measured using trypan exclusion counting and calculated in respect to control cells ($n = 3 \pm$ SD). * Denotes significant reduction in cell viability compared to the control cells with no treatment ($p < 0.05$).

would have undergone degradation inside the cartridge due to the high process temperature, the scaffolds, starting from their size, were characterized and studied according to the role they would play *in vivo*, once inserted into the surgical incision preceding lumpectomy or mastectomy.

Funding

This research received no external funding.

Declaration of Competing Interest

The authors declare that they have no known competing financial interests or personal relationships that could have appeared to influence the work reported in this paper.

Data availability

Data will be made available on request.

Appendix A. Supplementary data

Supplementary data to this article can be found online at https://doi.org/10.1016/j.ijpharm.2022.122363.

References

Affandi, B., Santoso, S.S.I., Djajadilaga, H.W., Moeloek, F.A., Prihartono, J., et al., 1987. Five-year experience with Norplant®. Contraception. 36 (4), 417–428.

Akram, M., Iqbal, M., Daniyal, M., Khan, A.U., 2017. Awareness and current knowledge of breast cancer. Biol. Res. 2 (50), 33.

Carneiro, B.A., El-Deiry, W.S., 2020. Targeting apoptosis in cancer therapy. Nat. Rev. Clin. Oncol. 17 (7), 395–417.

Corduas, F., Mathew, E., McGlynn, R., Mariotti, D., Lamprou, D.A., Mancuso, E., 2021. Melt-extrusion 3D printing of resorbable levofloxacin-loaded meshes: Emerging strategy for urogynaecological applications. Mater. Sci. Eng., C 1 (131), 112523.

Domínguez-Robles, J., Shen, T., Cornelius, V.A., Corduas, F., Mancuso, E., Donnelly, R.F., et al., 2021. Development of drug loaded cardiovascular prosthesis for thrombosis prevention using 3D printing. Mater. Sci. Eng., C 1 (129), 112375.

Espinoza SM, Patil HI, San Martin Martinez E, Casañas Pimentel R, Ige PP. Poly-ε-caprolactone (PCL), a promising polymer for pharmaceutical and biomedical applications: Focus on nanomedicine in cancer. Int J Polym Mater Polym Biomater. 2020 Jan 22;69(2):85–126.

Glover K, Mathew E, Pitzanti G, Magee E, Lamprou DA. 3D bioprinted scaffolds for diabetic wound-healing applications. Drug Deliv Transl Res [Internet]. 2022 Jan 11 [cited 2022 Sep 1]; Available from: https://doi.org/10.1007/s13346-022-01115-8.

Haume K, Rosa S, Grellet S, Śmiałek MA, Butterworth KT, Solov'yov AV, et al. Gold nanoparticles for cancer radiotherapy: a review. Cancer Nanotechnol. 2016 Nov 3;7 (1):8.

Hou, J., Li, C., Cheng, L., Guo, S., Zhang, Y., Tang, T., 2011. Study on hydrophilic 5-fluorouracil release from hydrophobic poly(ε-caprolactone) cylindrical implants. Drug Dev. Ind. Pharm. 37 (9), 1068–1075.

Hussain, S., Solanki, D., Yadav, R., 2021. Khan Y. An Overview, Implantable Drug Delivery System, p. 1.

Kean, T.J., Thanou, M., 2019. Utility of Chitosan for 3D Printing and Bioprinting. In: Crini, G., Lichtfouse, E. (Eds.), SusTaINablE AgRIculTuRE REvIEws 35: ChITIN ANd ChITosaN: HIsToRy, FuNdamENTals ANd INNovaTIoNs [INTERNET]. Springer International Publishing, Cham, pp. 271–292. https://doi.org/10.1007/978-3-030-16538-3_6. Sustainable Agriculture Reviews). Available from:

Kimura, Y., Okuda, H., 1999. Prevention by Chitosan of Myelotoxicity, Gastrointestinal Toxicity and Immunocompetent Organic Toxicity Induced by 5-Fluorouracil without Loss of Antitumor Activity in Mice. Jpn J Cancer Res Gann. 90 (7), 765–774.

Kleiner, L.W., Wright, J.C., Wang, Y., 2014. Evolution of implantable and insertable drug delivery systems. J. Control. Release 10 (181), 1–10.

Kus-Liśkiewicz, M., Fickers, P., Ben, T.I., 2021. Biocompatibility and Cytotoxicity of Gold Nanoparticles: Recent Advances in Methodologies and Regulations. Int. J. Mol. Sci. 22 (20), 10952.

Lovelace, D.L., McDaniel, L.R., Golden, D., 2019. Long-Term Effects of Breast Cancer Surgery, Treatment, and Survivor Care. J Midwifery Womens Health. 64 (6), 713–724.

Luderer, F., Begerow, I., Schmidt, W., Martin, H., Grabow, N., Bünger, C.M., et al., 2013. Enhanced visualization of biodegradable polymeric vascular scaffolds by incorporation of gold, silver and magnetite nanoparticles. J. Biomater. Appl. 28 (2), 219–231.

Mancuso, E., Shah, L., Jindal, S., Serenelli, C., Tsikriteas, Z.M., Khanbareh, H., et al., 2021. Additively manufactured BaTiO3 composite scaffolds: A novel strategy for load bearing bone tissue engineering applications. Mater. Sci. Eng., C 1 (126), 112192.

Mathew, E., Domínguez-Robles, J., Stewart, S.A., Mancuso, E., O'Donnell, K., Larrañeta, E., et al., 2019. Fused Deposition Modeling as an Effective Tool for Anti-Infective Dialysis Catheter Fabrication. ACS Biomater. Sci. Eng. 5 (11), 6300–6310.

Mathew, E., Pitzanti, G., Larrañeta, E., Lamprou, D.A., 2020. 3D Printing of Pharmaceuticals and Drug Delivery Devices. Pharmaceutics. 12 (3), 266.

Moo, T.A., Sanford, R., Dang, C., Morrow, M., 2018. Overview of Breast Cancer Therapy. PET Clin. 13 (3), 339–354.

Ortiz, R., Prados, J., Melguizo, C., Arias, J.L., Ruiz, M.A., Álvarez, P.J., et al., 2012. 5-Fluorouracil-loaded poly(ε-caprolactone) nanoparticles combined with phage E gene therapy as a new strategy against colon cancer. Int J Nanomedicine. 7, 95–107.

Radwan-Pragłowska, J., Piątkowski, M., Deineka, V., Janus, Ł., Korniienko, V., Husak, E., et al., 2019. Chitosan-Based Bioactive Hemostatic Agents with Antibacterial Properties—Synthesis and Characterization. Molecules 24 (14), 2629.

Ren, D., Yi, H., Wang, W., Ma, X., 2005. The enzymatic degradation and swelling properties of chitosan matrices with different degrees of N-acetylation. Carbohydr. Res. 340 (15), 2403–2410.

Rezaei, F.S., Khorshidian, A., Beram, F.M., Derakhshani, A., Esmaeili, J., Barati, A., 2021. 3D printed chitosan/polycaprolactone scaffold for lung tissue engineering: hope to be useful for COVID-19 studies. RSC Adv. 11 (32), 19508–19520.

Shrestha, S., Cooper, L.N., Antosh, M.P., 2016. Gold Nanoparticles for Radiation Enhancement in Vivo. Jacobs Jornal of radiation oncology. 3 (1).

Sternberg K, Petersen S, Grabow N, Senz V, Schwabedissen HM zu, Kroemer HK, et al. Implant-associated local drug delivery systems based on biodegradable polymers: customized designs for different medical applications. Biomed Tech Eng. 2013 Oct 1; 58(5):417–27.

Stewart, S.A., Domínguez-Robles, J., Donnelly, R.F., Larrañeta, E., 2018. Implantable Polymeric Drug Delivery Devices: Classification, Manufacture, Materials, and Clinical Applications. Polymers. 10 (12), 1379.

Stewart, S.A., Domínguez-Robles, J., McIlorum, V.J., Gonzalez, Z., Utomo, E., Mancuso, E., et al., 2020. Poly(caprolactone)-Based Coatings on 3D-Printed Biodegradable Implants: A Novel Strategy to Prolong Delivery of Hydrophilic Drugs. Mol. Pharm. 17 (9), 3487–3500.

Taghizadeh M, Taghizadeh A, Khodadadi Yazdi M, Zarrintaj P, J. Stadler F, D. Ramsey J, et al. Chitosan-based inks for 3D printing and bioprinting. Green Chem. 2022;24(1): 62–101.

Vines JB, Yoon JH, Ryu NE, Lim DJ, Park H. Gold Nanoparticles for Photothermal Cancer Therapy. Front Chem [Internet]. 2019 [cited 2022 May 28];7. Available from: https://www.frontiersin.org/article/10.3389/fchem.2019.00167.

Weaver, E., O'Hagan, C., Lamprou, D.A., 2022. The sustainability of emerging technologies for use in pharmaceutical manufacturing. Expert Opin Drug Deliv. 1–12.

Yang, Y., Wu, H., Fu, Q., Xie, X., Song, Y., Xu, M., et al., 2022. 3D-printed polycaprolactone-chitosan based drug delivery implants for personalized administration. Mater. Des. 1 (214), 110394.

Younes, I., Sellimi, S., Rinaudo, M., Jellouli, K., Nasri, M., 2014. Influence of acetylation degree and molecular weight of homogeneous chitosans on antibacterial and antifungal activities. Int. J. Food Microbiol. 18 (185), 57–63.